Observation of the Production of a W Boson in Association with a Single Charm Quark at the Tevatron

Lucio Cerrito, John Paul Chou, Melissa Franklin, Tony Liss, Shulamit Moed Sher

September 4, 2011

We present a measurement of the production cross section of a W boson in association with a single charm quark in $p\bar{p}$ collisions at $\sqrt{s} = 1.96$ TeV with the CDF detector. The analysis uses an integrated luminosity of 4.3 fb^{-1} and is based on the reconstruction of the final state with one high transverse-momentum electron or muon, missing transverse energy, and one hadronic jet. The signal is evinced by a charge asymmetry between the lepton from the W boson decay and a soft lepton from the semileptonic decay of the charm quark. We measure a production cross section times branching fraction of $13.3^{+3.3}_{-2.9}\,(\mathrm{stat} + \mathrm{syst})$ pb given a charm hadron with transverse momentum greater than 20 GeV and pseudorapidity within ± 1.5. This is consistent with the standard model expectation. Assuming a null hypothesis without the presence of the signal process, the number of events observed constitutes a $6.4\,\sigma$ excess.

Contents

1 Introduction

The production of a W boson in association with a single charm quark (W+c) proceeds at lowest order through sg and $\bar{s}g$ fusion. As can be seen Figs. 1 and 2, the electric charge of the lepton from the semileptonic decay of the charm quark and the electric charge of the lepton from the W boson decay are opposite in sign. We exploit this signature to distingush Wc events from the large background of other W+jet events, including W+c$\bar{\text{c}}$ and W+b$\bar{\text{b}}$. At the Tevatron, the W+c signal is approximately 5% of the inclusive W+1 jet cross section for jets with a transverse momentum greater than 10 GeV [1]. The production of W+c where the initial s quark is replaced by a d quark is suppressed by the CKM quark mixing matrix element V_{cd}. Given the larger d-quark partonic luminosity, this processes constitutes approximately 10% of the total production rate.

W+c production is a background process for several important physics signatures such as single-top production and associated W+Higgs production. It is also a significant component in the t$\bar{\text{t}}$ control region. Our motivation to perform this analysis is driven by the need to identify W+c events among W+heavy flavor events and to improve the understanding of backgrounds of the aforementioned processes. A CDF measurement of the W+c production cross section with soft muon tagging using ~ 1.8 fb^{-1} of data is reported in Ref. [2]. This note reports the measurements of the W+c production cross section using both soft electron and soft muon tagging, first separately, and then combined.

In the following section, we describe the measurement strategy. Section 3 describes the event selection and Sec. 4 describes the background estimation. The cross section result is presented in Sec. 5, with a full discussion of the systematic uncertainties and the combination technique. We present our conclusions in Sec. 7.

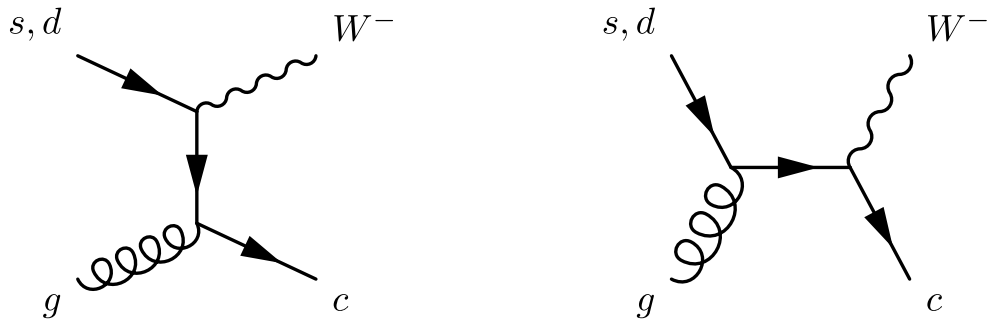

Figure 1: The leading order Feynman diagrams for W+charm production

2 Measurement Strategy

Our strategy is to select events in which the W boson decays leptonically, looking for a signature of one isolated, high p_{T} lepton due to the decay of a W boson, missing transverse energy ($\not\!\!E_{\text{T}}$), and one hadronic jet. To suppress multijet events, we require that the $\not\!\!E_{\text{T}}$ is greater than 25 GeV and the transverse mass of the lepton with the $\not\!\!E_{\text{T}}$ is greater than 20 GeV. We tag the jet by requiring that there is a soft electron or muon nearby.

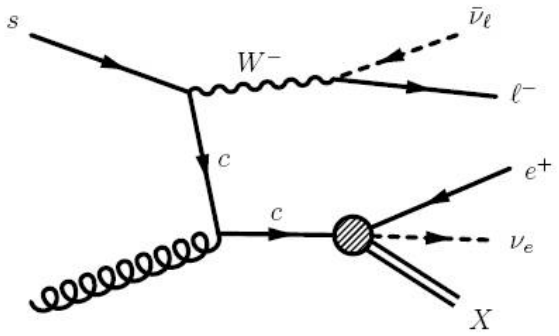

Figure 2: Feynman diagram of W plus single charm production with soft electron. When a soft muon is produced instead, the electron in the diagram final state is replaced by a muon.

We count the number of events where the charge of the lepton from the W and the soft lepton have opposite sign (OS) and same sign (SS). While the W+c signal has a strong OS–SS asymmetry, the background processes are mostly symmetric and/or very small. The dominant backgrounds to this process are events from W+jets, Z+jets and Drell–Yan, and multijet QCD. Some contributions from diboson production, single top, and $t\bar{t}$ are also present.

While the contribution from W+$b\bar{b}$ (W+$c\bar{c}$) is naively quite large and expected to dominate over any W+c signal, in fact it is nearly completely charge symmetric, since the soft lepton can come from either the b (c) or $\bar{b}$ ($\bar{c}$). Unlike W+jet events, contributions from Z+jets and Drell–Yan are strongly asymmetric. The contribution from these backgrounds is reduced with kinematic selections.

The W+c production cross section is proportional to the difference between the number of OS an SS events: $N_{\rm os} - N_{\rm ss}$. The cross section is calculated using the following formula:

$$\sigma = \frac{N^{\rm obs} - N^{\rm bkg}}{\epsilon \cdot S \cdot \mathcal{A} \cdot \int \mathcal{L}\, dt} \tag{1}$$

, where

- $N^{\rm obs}$ is the observed difference in the number of OS and SS events in data, $N^{\rm obs}_{\rm os} - N^{\rm obs}_{\rm ss}$,
- $N^{\rm bkg}$ is the expected difference in the number of OS and SS events due to the background, $N^{\rm bkg}_{\rm os} - N^{\rm bkg}_{\rm ss}$,
- ϵ is the difference in the efficiency to soft lepton tag W+c events,
- S is the OS–SS asymmetry in W+c events,
- $\mathcal{A}$ is the kinematic and geometrical acceptance of the event selection,
- $\int \mathcal{L}\, dt$ is integrated luminosity.

The W+jet backgrounds are estimated with data-driven techniques, described in subsequent sections. The estimate of the Z+jets and Drell–Yan backgrounds is determined from MC simulation and is cross-checked by looking at the event yields with different combinations of tight-lepton and

soft-lepton flavor, since these backgrounds are strongly suppressed in the cross-channels with different flavor leptons. The multijet background is estimated by fitting the $\not\!\!E_{\rm T}$ spectrum without the $\not\!\!E_{\rm T}$ requirement. An orthogonal sample of QCD-like events in the data is used to model the QCD shape.

The soft lepton taggers were validated and used previously in several CDF analyses. They are described in detail in Refs. [4, 5].

3 Event Selection and Datasets

The baseline selection for this measurement is based on the top group lepton+jets selection, where we ask for exactly one reconstructed jet:

- one isolated > 20 GeV CEM/CMUP/CMX lepton (the lepton flavor must be consistent with the trigger path);
- one > 20 GeV jet corrected to level 5 with $|\eta_D| < 2.0$, reconstructed with the R=0.4 JETCLU algorithm;
- $\not\!\!E_{\rm T} > 25$ GeV;
- veto cosmic ray muons, conversion electrons and Z bosons.

We additionally require that

- transverse mass of the isolated lepton and the $\not\!\!E_{\rm T}$, $M_{\rm T}$, is greater than 20 GeV;
- reject events when the invariant mass between the soft muon and tight muon is between 8–11 GeV or 70–110 GeV;
- reject events when the invariant mass between the soft electron and tight electron is greater than 45 GeV;
- reject events when the tight and soft leptons are both electrons and the difference in ϕ between the jet and $\not\!\!E_{\rm T}$ is less than 0.3.

These additional requirements are intended to further suppress multijet, Z+jet, and Drell–Yan events which are more prominent in this analysis than a typical top-quark analysis.

We tag the events by requiring the presence of a soft electron tag ($\rm SLT_e$) or a soft muon tag ($\rm SLT_\mu$) near the jet. The "nearness" requirement is that $\Delta R \leq 0.6$ for the $\rm SLT_\mu$ and $\Delta R \leq 0.4$ for the $\rm SLT_e$, where ΔR is the distance between the track and the jet-axis in η–ϕ space.

3.1 Data Sample

We use data through period 23. The data periods and their corresponding luminosities are summarized in Table 1. When requiring an $\rm SLT_\mu$, we find a total of 1482 OS events and 1024 SS events that satisfy the above selection criteria. Similarly, requiring an $\rm SLT_e$ yields 2494 OS and 2088 SS events. This corresponds to a difference of 458 events in the $\rm SLT_\mu$ channel, and 406 events in the $\rm SLT_e$ channel.

period	run range	dataset	luminosity (pb^{-1})		
			CEM	CMUP	CMX
0	13425-186598	bhel(mu)0d	331.47	331.47	318.11
1-4	190697-203799	bhel(mu)0h	362.94	362.94	359.5
5-7	203819-212133	bhel(mu)0i	258.37	258.37	258.37
8	217990-222426	bhel(mu)0i	166.29	166.29	166.29
9	222529-228596	bhel(mu)0i	156.76	156.76	152.78
10	228644-233111	bhel(mu)0i	243.19	243.19	243.49
11	233133-237795	bhel(mu)0j	234.99	234.99	229.98
12	237845-241664	bhel(mu)0j	162.01	162.01	155.25
13	241665-246231	bhel(mu)0j	280.86	280.86	268.35
14	25283-254686	bhel(mu)0k	32.01	32.01	30.59
15	254800-256824	bhel(mu)0k	161.87	161.87	156.36
16	256840-258787	bhel(mu)0k	101.81	101.81	100.74
17	258880-261005	bhel(mu)0k	183.56	183.56	182.93
18	261119-264071	bhel(mu)0m	304.88	295.85	304.99
19	264101-266513	bhel(mu)0m	206.98	206.98	206.99
20	266528-267718	bhel(mu)0m	226.92	226.9	226.9
21	268155-271047	bhel(mu)0m	435.59	435.57	435.58
22	271072-272214	bhel(mu)0m	265.67	265.67	265.67
23	272470-274055	bhel(mu)0m	200.65	200.68	200.68
total			4316.82	4307.78	4263.55

Table 1: Datasets used in this analysis and their corresponding luminosities.

3.2 Signal Sample

We simulate the W+c signal with a combination of ALPGEN for the event generation and PYTHIA for the showering (stopwX). In these samples, the charm quark is required to have $p_{\mathrm{T}} > 8$ GeV and $|\eta| < 3.0$ at the generator level. In order to provide a more robust cross-section measurement claim, we further restrict the charm quark to have $p_{\mathrm{T}} > 20$ GeV and $|\eta| < 1.5$. This also has the effect of minimizing the contribution from certain systematic uncertainties, such as the parton distribution functions.

Dataset names and cross sections for the different signal samples are listed in Table 2. Shown also is the leading order (LO) cross section times W$\rightarrow \ell\nu$ branching fraction for each process with the nominal charm selection. After requiring that the charm has $p_{\mathrm{T}} > 20$ GeV and $|\eta| < 1.5$, the inclusive cross section for the W($\rightarrow \ell\nu$)+c process is reduced from 21.1 pb to 7.5 pb.

We use MCMC to estimate an NLO K factor for this process of 1.5 ± 0.3, where the uncertainty is dominated by change in the K factor resulting from varying the renormalization and factorization scales up by a factor of 2 and down by a factor of 1/2. Therefore, we expect that the inclusive NLO W+c cross section times W$\rightarrow \ell\nu$ branching fraction is 11.3 ± 2.2 pb for a charm quark with $p_{\mathrm{T}} > 20$ GeV and $|\eta| < 1.5$.

process	sample	generator	cross section × BF
$W(e\nu)+c+0p$	stopw0	ALPGEN+PYTHIA	17.1 pb
$W(e\nu)+c+1p$	stopw1	ALPGEN+PYTHIA	3.39 pb
$W(e\nu)+c+2p$	stopw2	ALPGEN+PYTHIA	507 fb
$W(e\nu)+c+(3p)$	stopw3	ALPGEN+PYTHIA	83 fb
$W(\mu\nu)+c+0p$	stopw5	ALPGEN+PYTHIA	17.1 pb
$W(\mu\nu)+c+1p$	stopw6	ALPGEN+PYTHIA	3.39 pb
$W(\mu\nu)+c+2p$	stopw7	ALPGEN+PYTHIA	507 fb
$W(\mu\nu)+c\geq 3p$	stopw8	ALPGEN+PYTHIA	83 fb
$W(\tau\nu)+c+0p$	stopwa	ALPGEN+PYTHIA	17.1 pb
$W(\tau\nu)+c+1p$	stopwb	ALPGEN+PYTHIA	3.39 pb
$W(\tau\nu)+c+2p$	stopwc	ALPGEN+PYTHIA	507 fb
$W(\tau\nu)+c\geq 3p$	stopwd	ALPGEN+PYTHIA	83 fb

Table 2: Summary of the Monte Carlo W+single charm signal samples used in this analysis. The cross sections are multiplied by the leptonic branching fraction of the W boson, and require that the charm quark has $p_{\mathrm{T}} > 8$ GeV and $|\eta| < 3.0$.

4 Backgrounds

4.1 Monte Carlo Backgrounds

We estimate the backgrounds due to production of dibosons (WW, WZ, ZZ), single top, and $t\bar{t}$ from MC simulation. The contributions due to these processes are small, and the production cross sections are well-established. WW production contributes the most to the background among these processes and has a strong charge asymmetry because one lepton can be identified as the "W" lepton, while the other is the "soft" lepton. Interestingly, among these backgrounds, single-top processes contribute the second most to the $N_{\mathrm{os}} - N_{\mathrm{ss}}$, although the total contribution is quite small (less than two events, in either $\mathrm{SLT_e}$ or SLT_μ channel).

We expect 26.4 ± 2.8 SLT_μ events from these backgrounds, of which 17.5 ± 1.8 are OS and 8.9 ± 1.0 are SS. The dominant systematic uncertainties on these quantities are due to the luminosity and fake rate. The estimated OS–SS charge asymmetry is 0.33 ± 0.01.

Similarly, we expect 35.1 ± 3.5 $\mathrm{SLT_e}$ events, of which 27.7 ± 2.9 are OS and 7.4 ± 0.7 are SS; the charge asymmetry is 0.58 ± 0.01. The larger asymmetry is due to the fact that the second-lepton veto is less effective for electrons than for muons.

4.2 Drell–Yan and Z+jets events

Z+jets and Drell–Yan are distinguished in this analysis by the generator-level invariant-mass range of the dilepton pair. Events where $76 < M_{\ell\ell} < 106$ GeV are considered Z+jets, whereas events with dileptons pairs outside of this mass window are considered Drell–Yan.

The events for these processes are simulated with the ALPGEN + PYTHIA combination. Events with a $Z \to \tau\tau$ decay are simulated as well as $\mathrm{Z+b\bar{b}}$ and $\mathrm{Z+c\bar{c}}$ final states. The inclusive Z cross section times leptonic branching fraction calculated by ALPGEN is approximately 184 pb, whereas the

measured cross section is 264 ± 17 pb. We scale the simulated cross section to match the measured one. We then scale the cross section again by a factor of 1.2 ± 0.2 to account for the difference between the measured and predicted exclusive Z+1 jet cross section [6].

Events from these processes can enter the final selection through a number of means. The primary leptons from the Z-boson decay or the Drell–Yan process can be misidentified as a lepton from a W decay and a soft lepton. This results in a large charge asymmetry. Alternatively, only one primary lepton is reconstructed in the event, typically as the lepton from the W. The soft lepton results from the decay of heavy flavor or from 'fakes,' that is the mis-reconstruction of a hadronic track as a lepton.

We estimate 132 ± 30 SLT_{μ} events are due to Z+jets and Drell–Yan, of which 107 ± 24 are OS and 24 ± 6 are SS; the charge asymmetry is 0.63 ± 0.02. The asymmetry for Z+jets (~ 0.4) is much smaller than Drell–Yan (~ 0.9) because the Z vetos suppress events with a second leg in the Z-mass region and the second leg must come from fake muons. This is ineffective for Drell–Yan, and the asymmetry contribution is dominated by real off-shell Z legs.

Similarly, we estimate 138 ± 29 $\mathrm{SLT}_{\mathrm{e}}$ events, of which 87 ± 18 are OS and 51 ± 11 are SS. The charge asymmetry of 0.26 ± 0.01 is weaker than for SLT_{μ} because we place stricter requirements on the invariant mass of the electron–electron pair due to the bremsstrahlung tail. In both the $\mathrm{SLT}_{\mathrm{e}}$ and SLT_{μ} case, the dominant uncertainty on the event yield estimate comes from the cross section uncertainty.

4.3 Multijet QCD

Events due to multijet production can enter the event selection through hadronic mis-identification or heavy-flavor decay. Missing energy is the result of mis-measured jet energy, detector effects, as well as the occasional hard neutrino.

sample	$\mathrm{SLT}_{\mathrm{e}}$	SLT_{μ}
pretagged	$(3.3 \pm 0.5) \times 10^4$	$(3.9 \pm 0.6) \times 10^4$
OS-only tagged	201 ± 6	150 ± 8
SS-only tagged	173 ± 6	158 ± 9
OS−SS difference	27 ± 12	-8 ± 17

Table 3: The multijet QCD fractions for SLT_e and SLT_{μ} in the different samples, tagged and pretag events, and their corresponding uncertainties.

We estimate this background by releasing the $\not\!\!E_{\mathrm{T}}$ requirement on the events entirely and fitting the $\not\!\!E_{\mathrm{T}}$ spectrum using a binned, negative log-likelihood minimization, floating only the templates for the W+jets and multijet backgrounds. Meanwhile, the MC background templates are fixed. The contribution of the W+c signal is so small and the $\not\!\!E_{\mathrm{T}}$ distribution for W+c events is so similar to the W+jet events that we can confidently ignore the signal in the fit, allowing the W+jet background to cover the signal contribution.

Templates of the $\not\!\!E_{\mathrm{T}}$ variable are constructed out of simulation for all of the backgrounds except for the multijet background. The multijet template is constructed in data from an "anti-electron" sample, in which electron-triggered events are required to have an electron-like object which fails at least two selection criteria.

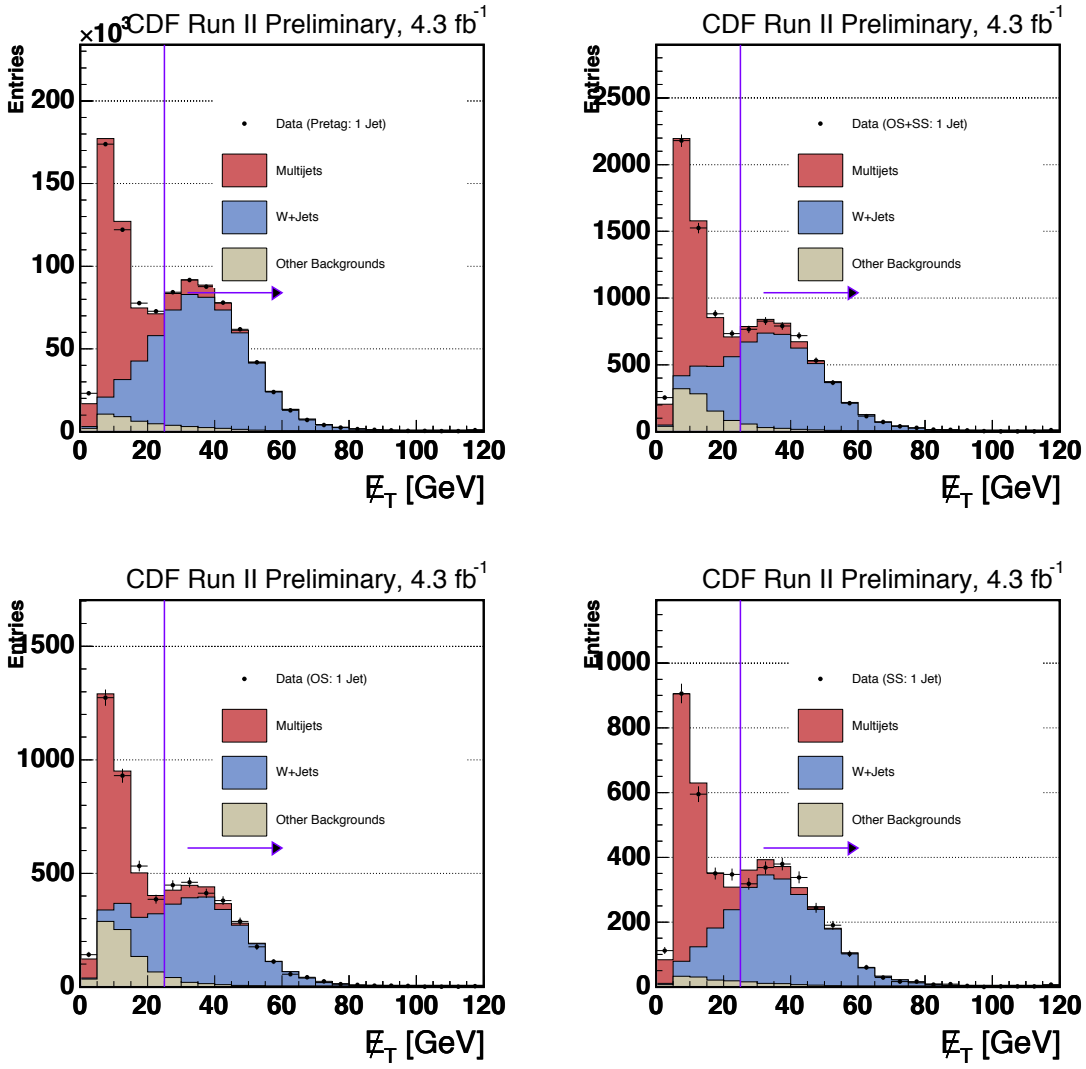

Figure 3: $\not\!\!E_{\rm T}$ distribution in the anti-electron sample for SLT$_e$ events, upper left plot - for pretag events, upper right plot - OS+SS events, lower left - OS events, lower right - SS events. The fit for this template, shown above, is used to determine the QCD fraction in our selection.

The $\not\!\!E_{\rm T}$ distribution in pretagged, OS-tagged, and SS-tagged events are fitted separately to determine the multijet content in each. The goodness-of-fit, as determined by a reduced-χ^2 test statistic, is very good (< 1.5) for the OS-tagged and SS-tagged fits. We assign a conservative 15% systematic uncertainty on the pretag fit result, but take the OS and SS estimates from the fit uncertainty inflated by the reduced-χ^2. Table 3 summarizes the event expectations from the multijet

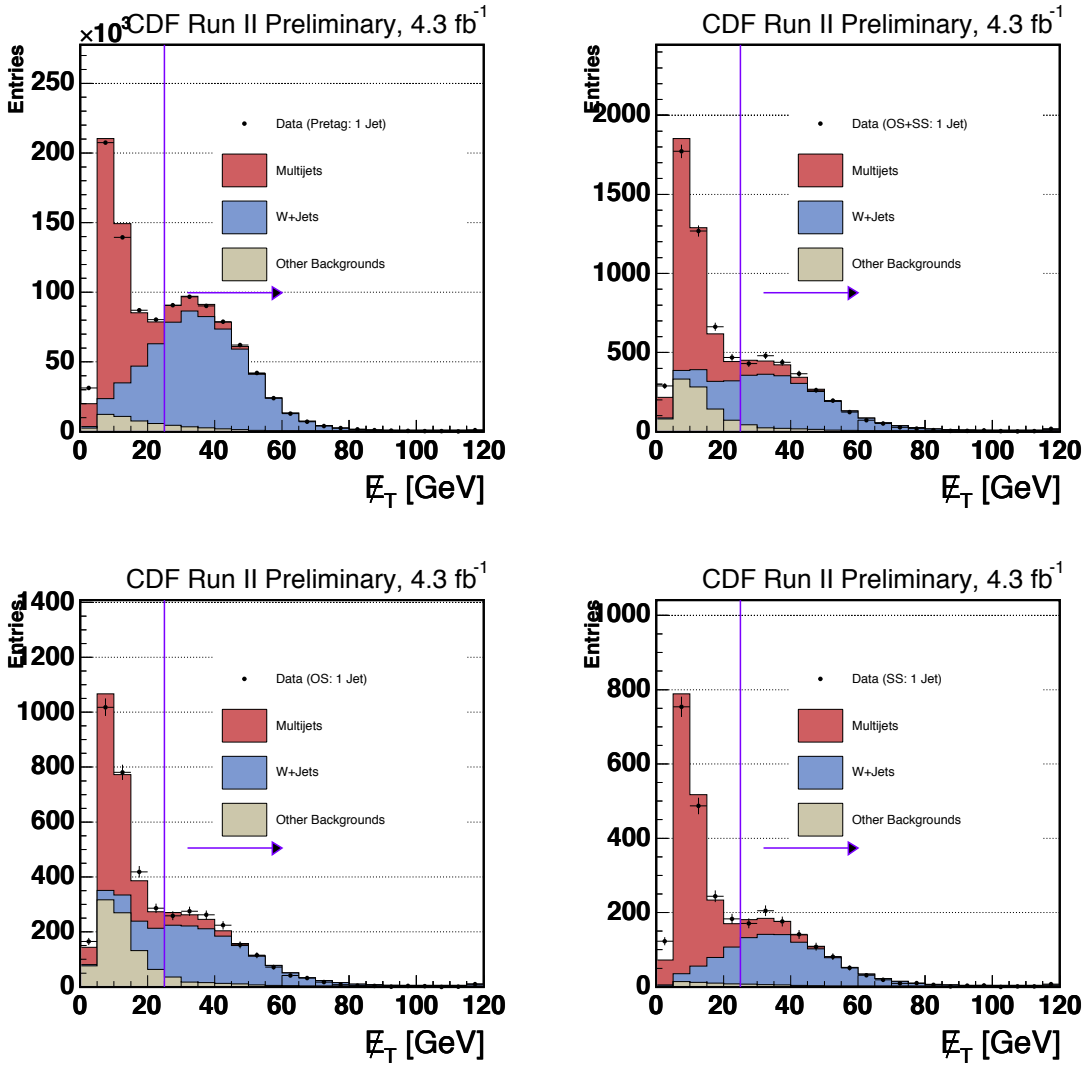

Figure 4: $\not\!\!E_{\rm T}$ distribution in the anti-electron sample for SLT$_\mu$ events, upper left plot - for pretag events, upper right plot - OS+SS events, lower left - OS events, lower right - SS events. The fit for this template, shown above, is used to determine the QCD fraction in our selection.

samples as determined by the fit results in the pretag, OS-only tagged, and SS-only tagged samples. We estimate the expected difference in OS$-$SS tags by simply subtracting one fit result from the other. The uncertainties in each fit are conservatively assumed to be fully correlated.

We measure a charge asymmetry for the multijet background of -0.03 ± 0.06 (SLT$_\mu$) and 0.07 ± 0.03 (SLT$_{\rm e}$). Figs. 3 and 4 show the fit results.

4.4 W + Jets

The dominant background to W+c production is the production of a W boson associated with jets. Rather than rely on a theoretical prediction of the production cross section, we estimate the contribution by normalizing the pretag yield to the data. We rely on a combination of MC and data-driven techniques to estimate the contribution to the tagged sample. The technique we use is similar to the "MethodII" [3] technique used to calculate the top cross section at CDF.

4.4.1 Pretag Estimate

The estimate of the number of pretag W+jet events is determined by subtracting off the pretag estimates of all other backgrounds and the signal from the total pretag event yield, that is:

$$N_{\rm pre}^{\rm W+jets} = N_{\rm pre}^{\rm data} - N_{\rm pre}^{\rm W+c} - N_{\rm pre}^{\rm MC} - N_{\rm pre}^{\rm Z+jets} - N_{\rm pre}^{\rm QCD}, \quad (2)$$

where the superscripts refer to the sample and the subscripts refer to the fact that these are the pretag expectations. In this case, W+jets does not include the W+c contribution typically associated with the process, but includes W+b$\bar{\rm b}$, W+c$\bar{\rm c}$, and W+light flavor. The superscript MC refers to all of the MC backgrounds (including WW production and single-top production), and Z+jets also includes Drell–Yan production.

In the SLT$_\mu$ analysis, we observe 516437 pretag events. We estimate that 12806 ± 794 are due to W+c, 1449 ± 93 are due to MC backgrounds, 14744 ± 2990 are due to Z+jets and Drell–Yan, and 39197 ± 5880 are due to QCD multijets. Here, the W+c pretag prediction is calculated assuming the nominal LO ALPGEN cross section, without correction. The W+jets pretag estimate is therefore 448242 ± 6815 events, which is dominated by the uncertainty on the QCD background. Similarly we observe 500618 pretag events for the SLT$_{\rm e}$ analysis, and we expect 440773 ± 5847 pretag W+jet events. We observe a slight difference in the pretag estimate in the two soft lepton tagger cases because we only apply the jet-$\not\!\!E_{\rm T}$ $\Delta\phi$ requirement in the SLT$_{\rm e}$ analysis, only. Table 4 summarizes the pretag contributions from each process for both SLT analyses.

process	# of events (SLT$_\mu$)	# of events (SLT$_{\rm e}$)	systematic source
diboson, single top, t$\bar{\rm t}$	1449 ± 93	1421 ± 91	luminosity
Z+Jets, Drell–Yan	14744 ± 2990	13296 ± 2699	cross section
QCD multijet	39197 ± 5880	32827 ± 4925	QCD fit
W+c	12806 ± 794	12301 ± 763	luminosity
W+b$\bar{\rm b}$, W+c$\bar{\rm c}$, W+l.f.	448242 ± 6815	440773 ± 5847	QCD fit
data	516437	500618	—

Table 4: Summary of pretag contributions from each process, including the dominant source of systematic uncertainties. Also shown is the number of pretag events observed in the data. The W+c contribution in this table assumes the cross section predicted by ALPGEN, not the final measured result. The W+b$\bar{\rm b}$, W+c$\bar{\rm c}$, and W+light flavor pretag prediction is determined by normalizing to the data.

4.4.2 Tag Estimate

We estimate the number of SLT tags via the equation,

$$N_{\rm tag}^{\rm W+jets} = N_{\rm pre}^{\rm W+jets}\left(\sum_i \epsilon_i^{\rm HF} F_i^{\rm HF} + \epsilon^{\rm LF}\left(1 - \sum_i F_i^{\rm HF}\right)\right), \quad (3)$$

where the ϵ's refer to the SLT efficiency for a given sample, and the $F^{\rm HF}$'s refer to the heavy flavor fraction for a given sample. The index i runs over the different heavy flavor configurations, which indicate whether the jet is matched to a parton-level hadron of type b or c. The heavy flavor fractions are determined from MC simulation. The heavy-flavor fractions are also corrected by a K factor of 1.4 ± 0.4, although this has a negligible effect on the final result. The fractions are $F_{\rm b}^{\rm HF} = (0.94 \pm 0.27)\%$ and $F_{\rm c}^{\rm HF} = (2.5 \pm 0.7)\%$, so the light flavor fraction is $1 - F_{\rm b}^{\rm HF} - F_{\rm c}^{\rm HF} = (96.6 \pm 0.7)\%$.

The SLT$_\mu$ heavy flavor efficiencies as measured in simulation are $\epsilon_{\rm b}^{\rm HF} = (3.5 \pm 0.2)\%$ and $\epsilon_{\rm c}^{\rm HF} = (1.6 \pm 0.1)\%$. The light flavor efficiency is measured directly in data by applying the fake rate to un-tagged tracks in the sample. The total number of tags predicted by the fake rate divided by the number of events in data is the estimate of $\epsilon^{\rm LF} = (0.34 \pm 0.006)\%$. Using Eq. 3, we expect 1808 ± 271 SLT$_\mu$ total W+jet events. The dominant uncertainty is due to the fake rate.

Similarly the SLT$_{\rm e}$ efficiencies as measured in simulation are $\epsilon^{\rm LF} = (0.89 \pm 0.07)\%$, $\epsilon_{\rm b}^{\rm HF} = (3.0 \pm 0.2)\%$, and $\epsilon_{\rm c}^{\rm HF} = (1.5 \pm 0.1)\%$. We estimate the SLT$_{\rm e}$ light flavor efficiency directly in simulation because of the non-trival component of photon conversion tags which would be uncounted using the same method as the SLT$_\mu$. Using Eq. 3, we expect 4076 ± 305 SLT$_\mu$ total W+jet events. The dominant uncertainty is due to the fake rate. We note that SLT$_{\rm e}$ fake efficiency is approximately twice that of the SLT$_\mu$, due to the higher fake rate at low $p_{\rm T}$ and extra contribution due to photon conversions. This results in roughly twice as many SLT$_{\rm e}$ tags as SLT$_\mu$ tags in the same sample.

process	# of events (SLT$_\mu$)	# of events (SLT$_{\rm e}$)	systematic source
diboson, single top, $t\bar{t}$	26 ± 3	35 ± 3	luminosity
Z+Jets, Drell–Yan	132 ± 30	138 ± 29	cross section
QCD multijet	308 ± 17	374 ± 12	QCD fit
W+c	214 ± 19	174 ± 16	luminosity
W+$b\bar{b}$, W+$c\bar{c}$, W+l.f.	1808 ± 271	4076 ± 305	fake rate
total expected	2488 ± 274	4797 ± 307	fake rate
data	2506	4582	—

Table 5: Summary of tag contributions from each process, including the dominant source of systematic uncertainties. Also shown is the number of tagged events observed in the data. The W+c contribution in this table assumes the cross section predicted by ALPGEN, not the final measured result. The overall agreement between predicted and observed tags is a consistency check of our method and demonstrates the reliability of our W+jet estimate in a control region.

Table 5 summarizes the total number of tags expected and measured in the data. We find good agreement in the number of predicted tags in both SLT channels. Since the primary component of the tagged sample is due to W+jet processes, this is a validation of the overall normalization due to this process. In the following section, we describe how we estimate the asymmetry due to W+jets.

4.4.3 Asymmetry Estimate

We measure the expected charge asymmetry for each process in MC simulation, except for the W+light flavor and QCD multijet backgrounds. For most backgrounds, the asymmetry is determined primarily through a real SLT. For instance, the charge of Z+jets is due principally to the dilepton decay, while there is some dilution of the asymmetry because of fake SLTs. Therefore, the charge asymmetry determination for this background in fact consists of measuring the ratio of real lepton tags (which have a nearly 100% asymmetry) to fake lepton tags (which have a close to 0% asymmetry). Photon conversions and other sources of tags complicate this picture, of course, but these are second order corrections. The procedures for measuring the contribution from real and fake lepton tags for both the SLT_μ and SLT_e are well-established and calibrated by a variety of means, not the least of which was the $t\bar{t}$ cross section measurement [7] and the $b\bar{b}$ validation of the SLT algorithms. Table 6 summarizes the asymmetry measurements for each background.

process	SLT_μ		SLT_e	
diboson, single top, $\mathrm{t\bar{t}}$	9 ± 1	0.33 ± 0.01	20 ± 2	0.58 ± 0.01
Z+Jets, Drell–Yan	84 ± 18	0.63 ± 0.02	36 ± 7	0.26 ± 0.01
QCD multijet	-8 ± 17	-0.03 ± 0.07	27 ± 12	0.07 ± 0.03
W+c	161 ± 13	0.75 ± 0.03	78 ± 7	0.45 ± 0.02
W+$\mathrm{b\bar{b}}$, W+$\mathrm{c\bar{c}}$, W+l.f.	86 ± 14	0.05 ± 0.01	174 ± 19	0.04 ± 0.01
total expected	331 ± 37	0.13 ± 0.02	336 ± 28	0.07 ± 0.01
data	458 ± 50	0.18 ± 0.02	406 ± 68	0.09 ± 0.01

Table 6: Summary of charge asymmety contributions from each process. The first column for each tagger consists of the expected number of OS−SS tags for that processes, and the second column consists of the expected asymmetry. Also shown is the observed result in the data, where the given errors reflect statistical uncertainties assuming an underlying Poisson process. The W+c contribution in this table assumes the cross section predicted by ALPGEN, not the final measured result. The difference between the observed and expected is interpreted as a underestimate of the W+c production cross section by the simulation.

Unlike most other backgrounds, the asymmetry in W+light flavor arises principally from fake lepton tags, where the leading hadron from the jet fragmentation preserves the electric charge of the underlying parton yielding a slight charge asymmetry with the lepton from the W boson. Simulation cannot be expected to model this perfectly, so a data-driven method must be pursued. We estimate the W+light flavor asymmetry from data by applying the fake matrix to un-tagged tracks. We expect that approximately 87–88% of the un-tagged sample is due to W+jets, while the rest are from other physics processes (see Table 4). The fake matrix predicts the probability that a given track will be tagged *assuming* that the track is a hadron. Therefore, this procedure should accurately estimate the asymmetry given the kinematics and geometry of the data sample.

Two points are worth making here. First, while the background contribution is small ($\sim 10\%$), it is not trivial. Fortunately, this method effectively suppresses contributions from the other background sources. If we want to arrive at the true asymmetry A_{LF} for W+light flavor events, then we

must correct the asymmetry that we measure A_m for the background components:

$$A_{\mathrm{LF}} = (1 + F) \cdot A_m - F \cdot A_x \tag{4}$$

where F is the fraction of events due to other sources (we stated it was about 10%) and A_x is the asymmetry of those sources. However, our estimate of A_x is also derived from the fake matrix itself, so its contribution must be of order A_m up to corrections for kinematic and geometric differences in the samples. In other words, because we apply the fake matrix to all un-tagged tracks, we are also applying them to, for instance, electrons from the decay of Z bosons. Although Z bosons have a high asymmetry, we are given those tracks the same (low) weight as if they were any other fake. Therefore, the correction to A_{LF} is only on order of the difference between the kinematics of real and fake electrons *times* the background fraction. Therefore, we expect that the effect of background contamination is much smaller than 10%.

Second, the application of the fake matrix is very important in predicting the charge asymmetry, particularly with respect to the kinematics of the candidate track. Tracks with high p_{T} in the W+light flavor sample have a much greater charge asymmetry than tracks with low p_{T}. This is because the high p_{T} tracks tend to preserve the charge of the underlying parton which undergoes fragmentation. On the other hand, tracks with high p_{T} have a much lower tagging probability than tracks with low p_{T}, an effect captured by the fake matrix. Only by convoluting these two effects correctly with the application of the fake matrix to the un-tagged data sample, can we accurately estimate the W+light flavor asymmetry.

Applying the SLT_μ (SLT_e) fake matrix to the un-tagged sample yields a W+light flavor asymmetry of 5.4% (5.4%). The agreement between these two numbers at this level is a numerical coincidence. Additionally, since the SLT_e fake matrix only estimates the tagging probability for hadrons, but not real electrons from conversions, we have not included the conversion contribution to the asymmetry. Because 21% of SLT_e tags are due to conversions, the W+light flavor asymmetry corrected for all contributions is 4.5%, assuming that conversions have an asymmetry identically equal to 0.

To calculate the total W+jets asymmetry (that is, including W+$\mathrm{b\bar{b}}$ and W+$\mathrm{c\bar{c}}$), we use the heavy flavor fractions and the W+heavy flavor tagging efficiencies to estimate the total contribution of OS−SS tags from W+heavy flavor. The contribution from these processes is symmetric at the few percent level, and contributes on the order of a few events to the total event count for either SLT. The SLT_μ (SLT_e) asymmetry for the entire W+jets process is 0.05 ± 0.01 (0.04 ± 0.01); equivalently, the number of OS tags minus SS tags expected due to W+jet events is 86 ± 13 (174 ± 19). The systematic uncertainty given here is dominated entirely by the fake rate.

5 Cross Section Measurement and Systematic Uncertainties

We interpret the excess of OS−SS events observed in the data over the background expectation as the production of W+c. Table 6 summarizes the observed number of events and expected number of events for each process. We use Eq. 1 to measure the W+c production cross section. The statistical uncertainty on the cross section is proportional to the square root of the total number of tagged events—opposite-sign plus same-sign. We estimate systematic uncertainties due to the SLT taggers, the luminosity, the assumed theoretical cross sections, the W lepton reconstruction and trigger efficiencies, and the QCD multijet fit for each background individually and propagate them to the cross section uncertainty algebraically. Additional uncertainties due to the jet energy scale,

initial- and final-state radiation, factorization and renormalization scales, hadronization modeling, and parton luminosity distributions are treated separately with a procedure to be discussed shortly.

We measure a production cross section for W+c where the charm parton has $p_{\mathrm{T}} > 20$ GeV and $|\eta| < 1.5$ of

$$\sigma = 13.4 \pm 2.3\,(\mathrm{stat}) \pm 2.4\,(\mathrm{syst}) \pm 1.1\,(\mathrm{lumi})\,\mathrm{pb}, \tag{5}$$

and

$$\sigma = 14.2 \pm 6.5\,(\mathrm{stat}) \pm 3.4\,(\mathrm{syst}) \pm 1.2\,(\mathrm{lumi})\,\mathrm{pb}, \tag{6}$$

for the SLT_{μ} and $\mathrm{SLT}_{\mathrm{e}}$ measurements, respectively.

As a cross check, we measure the W+c cross section separately in the e+jet and μ+jet final states. This also acts as a cross check of the Z+jet background estimate, because this background is suppressed in the e+SLT_{μ} and μ+$\mathrm{SLT}_{\mathrm{e}}$ channels. We find that

$$\sigma_{\mathrm{e},\mu} = 14.6 \pm 3.0\,(\mathrm{stat}) \pm 2.7\,(\mathrm{syst}) \pm 0.9\,(\mathrm{lumi})\,\mathrm{pb} \tag{7}$$

$$\sigma_{\mu,\mu} = 11.6 \pm 3.7\,(\mathrm{stat}) \pm 3.3\,(\mathrm{syst}) \pm 1.2\,(\mathrm{lumi})\,\mathrm{pb} \tag{8}$$

$$\sigma_{\mathrm{e,e}} = 12.1 \pm 9.6\,(\mathrm{stat}) \pm 4.0\,(\mathrm{syst}) \pm 1.2\,(\mathrm{lumi})\,\mathrm{pb} \tag{9}$$

$$\sigma_{\mu,\mathrm{e}} = 16.2 \pm 8.8\,(\mathrm{stat}) \pm 4.1\,(\mathrm{syst}) \pm 1.2\,(\mathrm{lumi})\,\mathrm{pb}, \tag{10}$$

where the first index refers to the lepton flavor from the W boson decay, and the second index refers to the lepton flavor of the SLT. As the statistical uncertainty in each of these measurements is independent, we note that they all give a consistent measurement of the W+c cross section. The same-flavor cross-section measurements are consistently lower than the opposite-flavor measurements. Although this is consistent with a slight over-estimate of the Z+jet and Drell–Yan backgrounds, there is little to suggest a faulty estimate.

We estimate the effect of the jet-energy scale on the acceptance calculation by varying the jet-energy correction $\pm 1\sigma$ about its uncertainties. We find that acceptance varies 2.0% as a result, which we apply as a systematic uncertainty on our cross section measurement. To measure the effect of initial-state and final-state radiation (ISR/FSR), we measure the W+jet acceptance in different samples with the ISR/FSR increased and decreased coherently. This has a 6% overall effect on the acceptance. Similarly, we vary the factorization and renormalization scales Q^2 up and down by a factor of 2.0 and 0.5, respectively, in the W+c simulation. We find a 1.3% overall effect on the acceptance.

We quote a systematic uncertainty of 4.6% on the simulation of the jet hadronization. This is done by swapping out the PYTHIA shower modeling for HERWIG in a sample similar to the W+c samples (see Ref [2] for details). PDF uncertainties are computed by remeasuring the acceptance with different PDFsets. We add all systematic uncertainties together in quadrature. The relative contribution from each is quoted in Table 7. The dominant systematics in this measurement are due to uncertainties surrounding the SLTs, the factorization and renormalization scales, the luminosity, and the uncertainty on the QCD multijet fit.

6 Combination

We combine the results from the two SLT taggers by performing a profile likelihood minimization. Systematic uncertainties are assumed to be either 100% correlated if they are shared between the two taggers or 0% correlated if not. We assume Wilks' theorem in establishing a 68% confidence

source	uncertainty (%) SLT_μ	SLT_e
SLT uncertainties	9.2	16.6
Factorization/Renormalization scales	1.3	
Luminosity	7.9	8.3
QCD multijet fit	6.3	9.9
ISR/FSR	6.0	
background cross sections	5.7	4.7
PDFs	3.6	
W-lepton ID	2.2	
Jet-energy scale	2.0	
Total	16.7	22.9

Table 7: Source of systematic uncertainties for the measurement ordered by relative size. The total systematic uncertainty is taken as the quadrature sum of the individual sources.

interval by determining for which values of the cross section the negative log likelihood increases by half a unit. The combined measured value of the cross section times leptonic branching fraction is $13.3^{+3.3}_{-2.9}\,(\mathrm{stat}+\mathrm{syst})$ pb for a charm hadron $p_\mathrm{T} > 20$ GeV and $|\eta| < 1.5$. Figure 5 shows twice the negative log likelihood ($-2\log\lambda(\sigma_\mathrm{Wc})$) as a function of the cross section. We note that the central value of the combined cross section is lower than either the SLT_e or SLT_μ measurements. This is due to the asymmetric error reporting. If we were to symmetrize the uncertainties, the central value of 13.5 pb would then lie between the two measurements.

In the case of the null hypothesis where the signal cross section times branching fraction vanishes, the value of $\sqrt{-2\log\lambda(\sigma_\mathrm{Wc} = 0\ \mathrm{pb})}$ is $6.4\,\sigma$. We interpret this to be the first observation of W+c production at the Tevatron.

7 Conclusions

We have performed a measurement of the production cross section of a W boson in association with a single charm quark in $\mathrm{p\bar{p}}$ collisions at $\sqrt{s} = 1.96$ TeV with the CDF detector. The analysis uses an integrated luminosity of 4.3 fb^{-1} and is based on the reconstruction of the final state with one high transverse-momentum electron or muon, missing transverse energy, and one hadronic jet. We measure a production cross section times branching fraction of $13.3^{+3.3}_{-2.9}\,(\mathrm{stat}+\mathrm{syst})$ pb given a charm hadron with transverse momentum greater than 20 GeV and $|\eta| < 1.5$. This is consistent with the theoretical NLO production cross section times branching fraction of 11.3 ± 2.2 pb, but it is in tension with a LO production cross section times branching fraction of 7.5 ± 1.5 pb. Assuming a null hypothesis without the presence of the signal process, the number of events observed constitutes a $6.3\,\sigma$ excess.

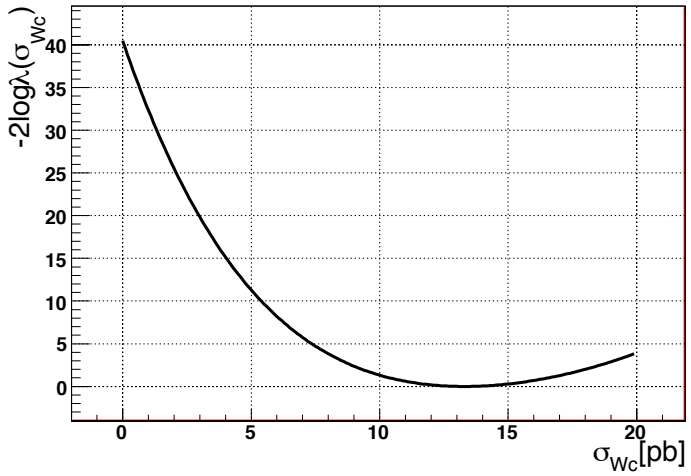

Figure 5: Twice the negative log likelihood as a function of the cross section. The minimum corresponds to the central value.

References

[1] hep-ph/9308370; U. Baur, F. Halzen, S. Keller, M.L. Mangano, K. Riesselmann

[2] CDF note 8026, A. Abulencia, L. Cerrito, U. Grundler, T. Liss, X. Zhang, "First measurement of the Wc production cross-section with SLT flavor tagging".

[3] CDF note 9185, J. Adelman *et al*, "Method II For You".

[4] L. Cerrito, A. Taffard, CDF note 6305 "A Soft Muon Tagger for Run II", CDF note 7122 "A Soft Muon Tagger for Run II: Summer-04 version"

[5] John Paul Chou, CDF note 9603 "ttbar Production Cross Section Measurement using Soft Electron Tagging in ppbar Collisions", SLT_e CDF notes 8787-8790

[6] CDF note 9161, M. Franklin *et al*, "Updated Search for the Flavor Changing Neutral Current Decay t -¿ Zq with 1.9/fb of CDF-II Data"

[7] John Paul Chou Phd thesis, http://huhepl.harvard.edu/theses/chou.pdf

[8] PRL 105:101801, 2010 ; Phys.Rev.D 81:092002, 2010

[9] CDF note 6894. "Track Reconstruction Efficiency in Jets".

[10] A. D. Martin,R. G. Roberts, W. J. Stirling, and R. S. Thorne, Eur. Phys. J. C 4, 463 (1998)

APPENDIX

A Background Samples

process	sample	generator	(cross section)* (Branching Fraction)
WW	itopww	PYTHIA	12.4 +/- 0.8 pb
WZ	itopwz	PYTHIA	3.7 +/- pb
ZZ	itopzz	PYTHIA	3.8 +/- 0.4 pb
single top s-channel, $M_t = 175$ GeV	stop00	MadEvent+PYTHIA	
single top t-channel LO, $M_t = 175$ GeV	stop01	MadEvent+PYTHIA	
$t\bar{t}$, M_t=175 GeV	ttop75	PYTHIA	
$W(e\nu) + c + 0p$	stopw0	ALPGEN+PYTHIA	17.1 pb
$W(e\nu) + c + 1p$	stopw1	ALPGEN+PYTHIA	3.39 pb
$W(e\nu) + c + 2p$	stopw2	ALPGEN+PYTHIA	507 fb
$W(e\nu) + c + (3p)$	stopw3	ALPGEN+PYTHIA	83 fb
$W(\mu\nu) + c + 0p$	stopw5	ALPGEN+PYTHIA	17.1 pb
$W(\mu\nu) + c + 1p$	stopw6	ALPGEN+PYTHIA	3.39 pb
$W(\mu\nu) + c + 2p$	stopw7	ALPGEN+PYTHIA	507 fb
$W(\mu\nu) + c \geq 3p$	stopw8	ALPGEN+PYTHIA	83 fb
$W(e\nu) + 0p$	ptopw0	ALPGEN+PYTHIA	1.80 nb
$W(e\nu) + 1p$	ptopw1	ALPGEN+PYTHIA	225 pb
$W(e\nu) + 2p$	ptop2w	ALPGEN+PYTHIA	35.3 pb
$W(e\nu) + 3p$	ptop3w	ALPGEN+PYTHIA	5.59 pb
$W(e\nu) + (4p)$	ptop4w	ALPGEN+PYTHIA	1.03 pb
$W(\mu\nu) + 0p$	ptopw5	ALPGEN+PYTHIA	1.80 nb
$W(\mu\nu) + 1p$	ptopw6	ALPGEN+PYTHIA	225 pb
$W(\mu\nu) + 2p$	ptop7w	ALPGEN+PYTHIA	35.3 pb
$W(\mu\nu) + 3p$	ptop8w	ALPGEN+PYTHIA	5.59 pb
$W(\mu\nu) + (4p)$	ptop9w	ALPGEN+PYTHIA	1.03 pb
$W(e\nu) + cc + 0p$	ctop0w	ALPGEN+PYTHIA	5.00 pb
$W(e\nu) + cc + 1p$	ctop1w	ALPGEN+PYTHIA	1.79 pb
$W(e\nu) + cc + (2p)$	ctop2w	ALPGEN+PYTHIA	0.628 pb
$W(\mu\nu) + cc + 0p$	ctop5w	ALPGEN+PYTHIA	5.00 pb

Table 8: Summary of the Monte Carlo background samples used in this analysis.

B Kinematic Plots

process	sample	generator	(cross section)* (Branching Fraction)
$W(\mu\nu) + cc + 1p$	ctop6w	ALPGEN+PYTHIA	1.79 pb
$W(\mu\nu) + cc + (2p)$	ctop7w	ALPGEN+PYTHIA	0.628 pb
$W(e\nu) + b\bar{b} + 0p$	btop0w	ALPGEN+PYTHIA	2.98 pb
$W(e\nu) + b\bar{b} + 1p$	btop1w	ALPGEN+PYTHIA	0.888 pb
$W(e\nu) + b\bar{b} + (2p)$	btop2w	ALPGEN+PYTHIA	0.287 pb
$W(mu\nu) + b\bar{b} + 0p$	btop5w	ALPGEN+PYTHIA	2.98 pb
$W(mu\nu) + b\bar{b} + 1p$	btop6w	ALPGEN+PYTHIA	0.889 pb
$W(mu\nu) + b\bar{b} + (2p)$	btop7w	ALPGEN+PYTHIA	0.286 pb
$W(\tau\nu) + c + 0p$	stopwa	ALPGEN+PYTHIA	17.1 pb
$W(\tau\nu) + c + 1p$	stopwb	ALPGEN+PYTHIA	3.39 pb
$W(\tau\nu) + c + 2p$	stopwc	ALPGEN+PYTHIA	507 fb
$W(\tau\nu) + c + (3p)$	stopwd	ALPGEN+PYTHIA	83.0 fb
$Z(ee) + 2p$ mZ=[75,105]GeV	ztop2p	ALPGEN+PYTHIA	3.47 pb
$Z(ee) + 3p$ mZ=[75,105]GeV	ztop3p	ALPGEN+PYTHIA	0.550 pb
$Z(ee) + (4p)$ mZ=[75,105]GeV	ztop4p	ALPGEN+PYTHIA	99.2 fb
$Z(\mu\mu) + 2p$ mZ=[75,105]GeV	ztop7p	ALPGEN+PYTHIA	3.47 pb
$Z(\mu\mu) + 3p$ mZ=[75,105]GeV	ztop8p	ALPGEN+PYTHIA	0.548 pb
$Z(\mu\mu) + (4p)$ mZ=[75,105]GeV	ztop9p	ALPGEN+PYTHIA	99.2 fb
$Z(ee) + b\bar{r} + 0p$ mZ=[75,105]GeV	ztopb0	ALPGEN+PYTHIA	511 fb
$Z(ee) + b\bar{r} + 1p$ mZ=[75,105]GeV	ztopb1	ALPGEN+PYTHIA	134 fb
$Z(ee) + b\bar{r} + (2p)$ mZ=[75,105]GeV	ztopb2	ALPGEN+PYTHIA	38.5 fb
$Z(\mu\mu) + b\bar{r} + 0p$ mZ=[75,105]GeV	ztopb5	ALPGEN+PYTHIA	511 fb
$Z(\mu\mu) + b\bar{r} + 1p$ mZ=[75,105]GeV	ztopb6	ALPGEN+PYTHIA	134 fb
$Z(\mu\mu) + b\bar{r} + (2p)$ mZ=[75,105]GeV	ztopb7	ALPGEN+PYTHIA	38.5 fb
$Z(\tau\tau) + b\bar{r} + (0p)$ mZ=[75,105]GeV	ztopbt	ALPGEN+PYTHIA	625 fb
$Z(ee) + cc + 0p$ mZ=[75,105]GeV	ztopc0	ALPGEN+PYTHIA	1.08 pb
$Z(ee) + cc + 1p$ mZ=[75,105]GeV	ztopc1	ALPGEN+PYTHIA	331 fb
$Z(ee) + 0p$ mZ=[75,105]GeV	ztopp0	ALPGEN+PYTHIA	158 pb
$Z(ee) + 1p$ mZ=[75,105]GeV	ztopp1	ALPGEN+PYTHIA	21.6 pb
$Z(\mu\mu) + 0p$ mZ=[75,105]GeV	ztopp5	ALPGEN+PYTHIA	158 pb
$Z(\mu\mu) + 1p$ mZ=[75,105]GeV	ztopp6	ALPGEN+PYTHIA	21.6 pb
$Z(\tau\tau) + (2p)$ mZ=[75,105]GeV	ztopt2	ALPGEN+PYTHIA	4.14 pb
$Z(tau\tau) + 0p$ mZ=[75,105]GeV	ztopt3	ALPGEN+PYTHIA	158 pb
$Z(tau\tau) + 1p$ mZ=[75,105]GeV	ztopt4	ALPGEN+PYTHIA	21.5 pb
$Z(ee) + cc + (2p)$ mZ=[75,105]GeV	ztopc2	ALPGEN+PYTHIA	107 fb
$Z(\mu\mu) + cc + 0p$ mZ=[75,105]GeV	ztopc5	ALPGEN+PYTHIA	1.08 pb
$Z(\mu\mu) + cc + 1p$ mZ=[75,105]GeV	ztopc6	ALPGEN+PYTHIA	332 fb
$Z(\mu\mu) + cc + (2p)$ mZ=[75,105]GeV	ztopc7	ALPGEN+PYTHIA	107 fb
$Z(\tau\tau) + cc + (0p)$ mZ=[75,105]GeV	ztopct	ALPGEN+PYTHIA	1.28 pb
$t\bar{t}$ w/ ISR,FSR "more"; M_t=175 GeV	otop03	PYTHIA	1514 pb
$t\bar{t}$ w/ ISR,FSR "less"; M_t=175 GeV	otop04	PYTHIA	1514 pb
$t\bar{t}$ M_t=172.5 GeV	ytkt72	PYTHIA	1514 pb

Table 9: Summary of the Monte Carlo background samples used in this analysis.

process	sample	generator	(cross section)* (Branching Fraction)
$DY(ee) + 0p$ mZ=[20,75]GeV	xtop0p	ALPGEN+PYTHIA	160 pb
$DY(ee) + 1p$ mZ=[20,75]GeV	xtop1p	ALPGEN+PYTHIA	8.39 pb
$DY(ee) + 2p$ mZ=[20,75]GeV	xtop2p	ALPGEN+PYTHIA	1.61 pb
$DY(ee) + 3p$ mZ=[20,75]GeV	xtop3p	ALPGEN+PYTHIA	233 fb
$DY(ee) + (4p)$ mZ=[20,75]GeV	xtop4p	ALPGEN+PYTHIA	39.8 fb
$DY(\mu\mu) + 0p$ mZ=[20,75]GeV	xtop5p	ALPGEN+PYTHIA	160 pb
$DY(\mu\mu) + 1p$ mZ=[20,75]GeV	xtop6p	ALPGEN+PYTHIA	8.40 pb
$DY(\mu\mu) + 2p$ mZ=[20,75]GeV	xtop7p	ALPGEN+PYTHIA	1.60 pb
$DY(\mu\mu) + 3p$ mZ=[20,75]GeV	xtop8p	ALPGEN+PYTHIA	233 fb
$DY(\mu\mu) + (4p)$ mZ=[20,75]GeV	xtop9p	ALPGEN+PYTHIA	39.8 fb
$DY(\tau\tau) + 0p$ mZ=[20,75]GeV	xtopt0	ALPGEN+PYTHIA	160 pb
$DY(\tau\tau) + 0p$ mZ=[20,75]GeV	xtopt1	ALPGEN+PYTHIA	8.38 pb
$DY(\tau\tau) + (2p)$ mZ=[20,75]GeV	xtopt2	ALPGEN+PYTHIA	1.82 pb
$DY(ee) + 0p$ mZ=[105,600]GeV	ytop0p	ALPGEN+PYTHIA	4.07 pb
$DY(ee) + 1p$ mZ=[105,600]GeV	ytop1p	ALPGEN+PYTHIA	706 fb
$DY(ee) + 2p$ mZ=[105,600]GeV	ytop2p	ALPGEN+PYTHIA	117 fb
$DY(ee) + 3p$ mZ=[105,600]GeV	ytop3p	ALPGEN+PYTHIA	18.5 fb
$DY(ee) + (4p)$ mZ=[105,600]GeV	ytop4p	ALPGEN+PYTHIA	3.33 fb
$DY(\mu\mu) + 0p$ mZ=[105,600]GeV	ytop5p	ALPGEN+PYTHIA	4.07 pb
$DY(ee) + 1p$ mZ=[105,600]GeV	ytop6p	ALPGEN+PYTHIA	706 fb
$DY(ee) + 2p$ mZ=[105,600]GeV	ytop7p	ALPGEN+PYTHIA	117 fb
$DY(ee) + 3p$ mZ=[105,600]GeV	ytop8p	ALPGEN+PYTHIA	18.5 fbb
$DY(\mu\mu) + (4p)$ mZ=[105,600]GeV	ytop9p	ALPGEN+PYTHIA	3.32 fb
$DY(ee) + 0p$ mZ=[8,20]GeV	ztopl0	ALPGEN+PYTHIA	1514 pb
$DY(ee) + 1p$ mZ=[8,20]GeV	ztopl1	ALPGEN+PYTHIA	19.7 pb
$DY(ee) + 2p$ mZ=[8,20]GeV	ztopl2	ALPGEN+PYTHIA	6.98 pb
$DY(\mu\mu) + 0p$ mZ=[8,20]GeV	ztopm0	ALPGEN+PYTHIA	1514 pb
$DY(\mu\mu) + 1p$ mZ=[8,20]GeV	ztopm1	ALPGEN+PYTHIA	19.7 pb
$DY(\mu\mu) + 2p$ mZ=[8,20]GeV	ztopm2	ALPGEN+PYTHIA	6.98 pb
$W(e\nu) + c >= 0p$	stopwe	ALPGEN+PYTHIA	17.1 pb
$W(e\nu) + c >= 0p$ Less FSR	stopwf	ALPGEN+PYTHIA	17.1 pb
$W(e\nu) + c >= 0p$ More FSR	stopwg	ALPGEN+PYTHIA	17.1 pb
$W(\mu\nu) + c >= 0p$	stopwh	ALPGEN+PYTHIA	17.1 pb
$W(\mu\nu) + c >= 0p$ Less FSR	stopwi	ALPGEN+PYTHIA	17.1 pb
$W(\mu\nu) + c >= 0p$ More FSR	stopwj	ALPGEN+PYTHIA	17.1 pb
$W(e\nu) + c >= 0p$ Less ISR	stopwn	ALPGEN+PYTHIA	21.7 pb
$W(e\nu) + c >= 0p$ More ISR	stopwo	ALPGEN+PYTHIA	21.7 pb
$W(\mu\nu) + c >= 0p$ Less ISR	stopwp	ALPGEN+PYTHIA	21.7 pb
$W(\mu\nu) + c >= 0p$ More ISR	stopwq	ALPGEN+PYTHIA	21.74 pb
$W(e\nu) + c + 0p$ Q^2 Sys	ctopq0	ALPGEN+PYTHIA	23.3 pb pb
$W(e\nu) + c + 1p$ Q^2 Sys	ctopq1	ALPGEN+PYTHIA	5.2 pb pb
$W(e\nu) + c + 2p$ Q^2 Sys	ctopq2	ALPGEN+PYTHIA	1.02 pb
$W(e\nu) + c + 3p$ Q^2 Sys	ctopq3	ALPGEN+PYTHIA	0.19 pb
$W(e\nu) + c + 0p$ Q^2 Sys	ctopq4	ALPGEN+PYTHIA	23.3 pb
$W(e\nu) + c + 1p$ Q^2 Sys	ctopq5	ALPGEN+PYTHIA	5.2 pb
$W(e\nu) + c + 2p$ Q^2 Sys	ctopq6	ALPGEN+PYTHIA	1.02 pb
$W(e\nu) + c + 3p$ Q^2 Sys	ctopq7	ALPGEN+PYTHIA	0.19 pb
$W(e\nu) + c >= 0p$ Less ISR	stopwn	ALPGEN+PYTHIA	21.7 pb

Table 10: Summary of the Monte Carlo background samples used in this analysis.

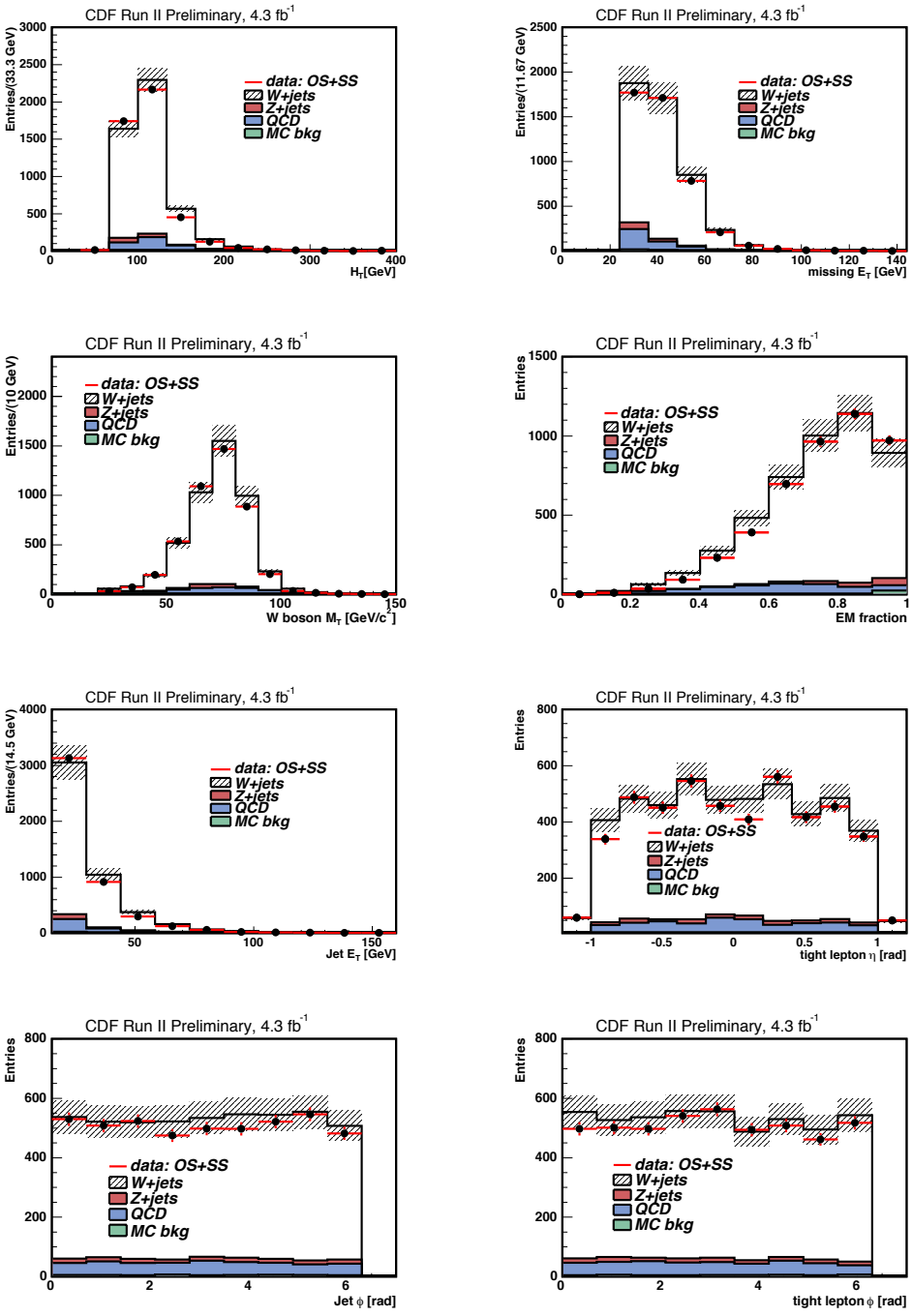

Figure 6: Kinematic plots of events tagged with the $\mathrm{SLT_e}$. Each bin contains the sum of opposite-sign and same-sign events.

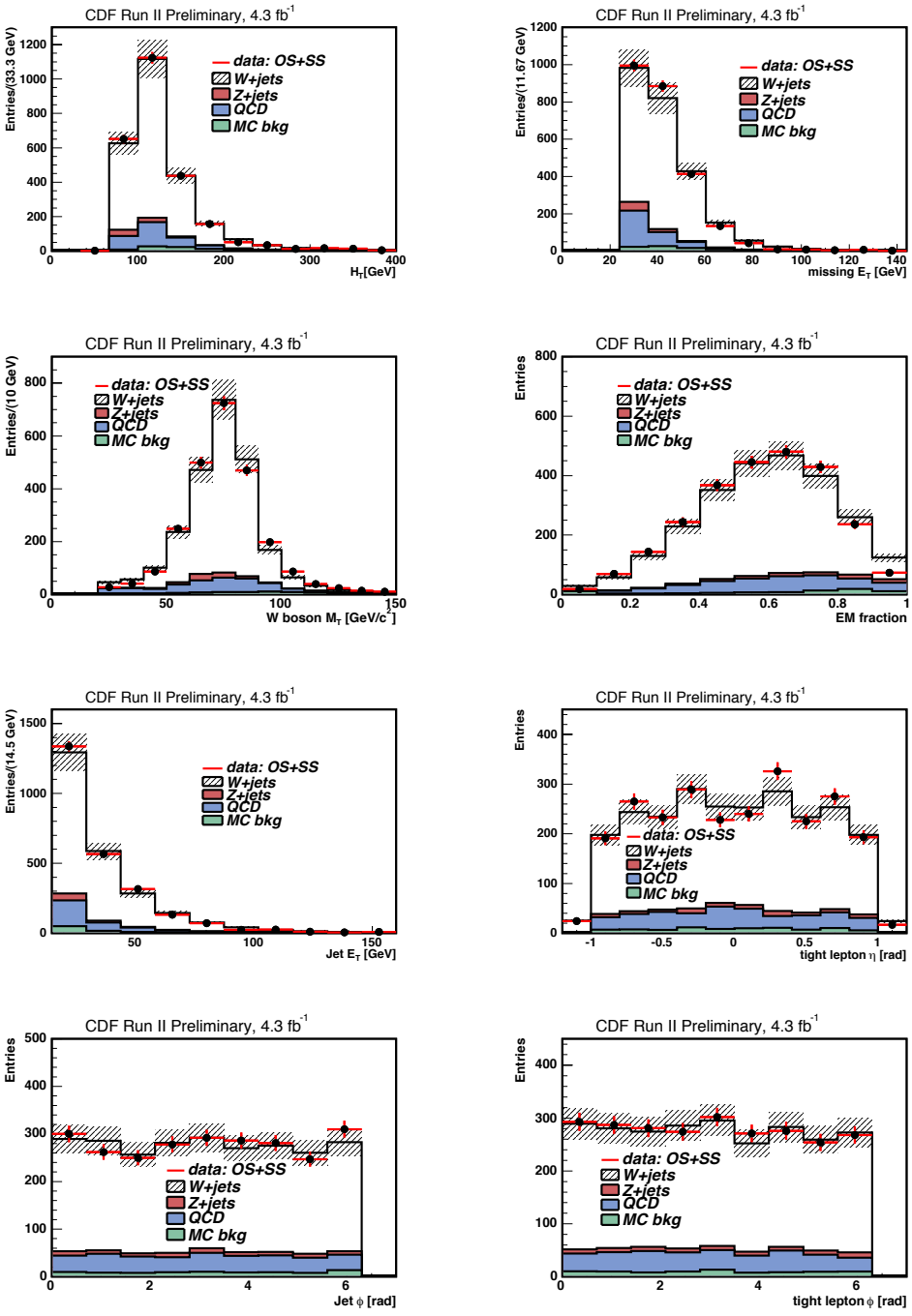

Figure 7: Kinematic plots of events tagged with the SLT$_\mu$. Each bin contains the sum of opposite-sign and same-sign events.

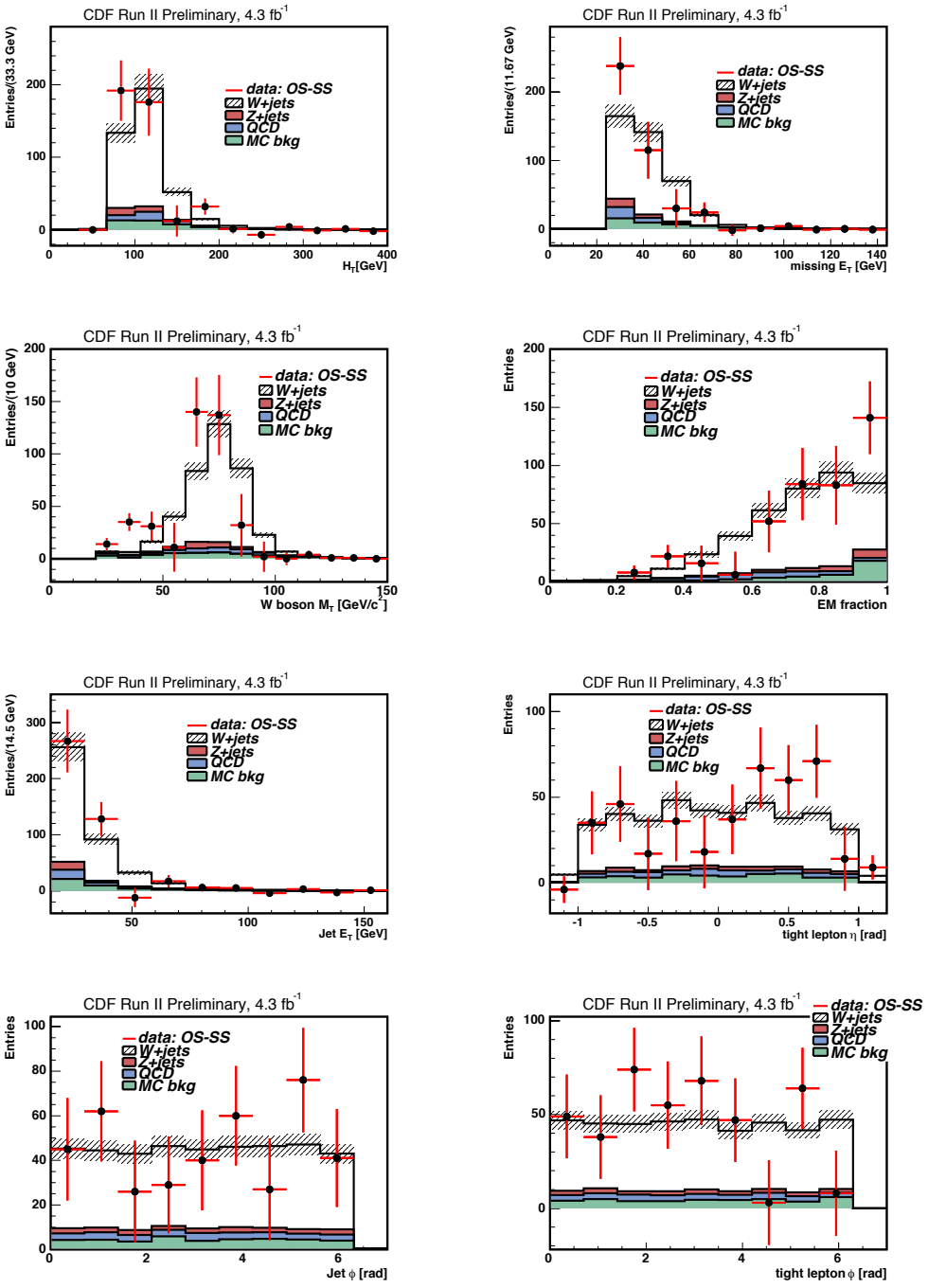

Figure 8: Kinematic plots of events tagged with the SLT_e. Each bin contains the difference between the number of opposite-sign and same-sign events.

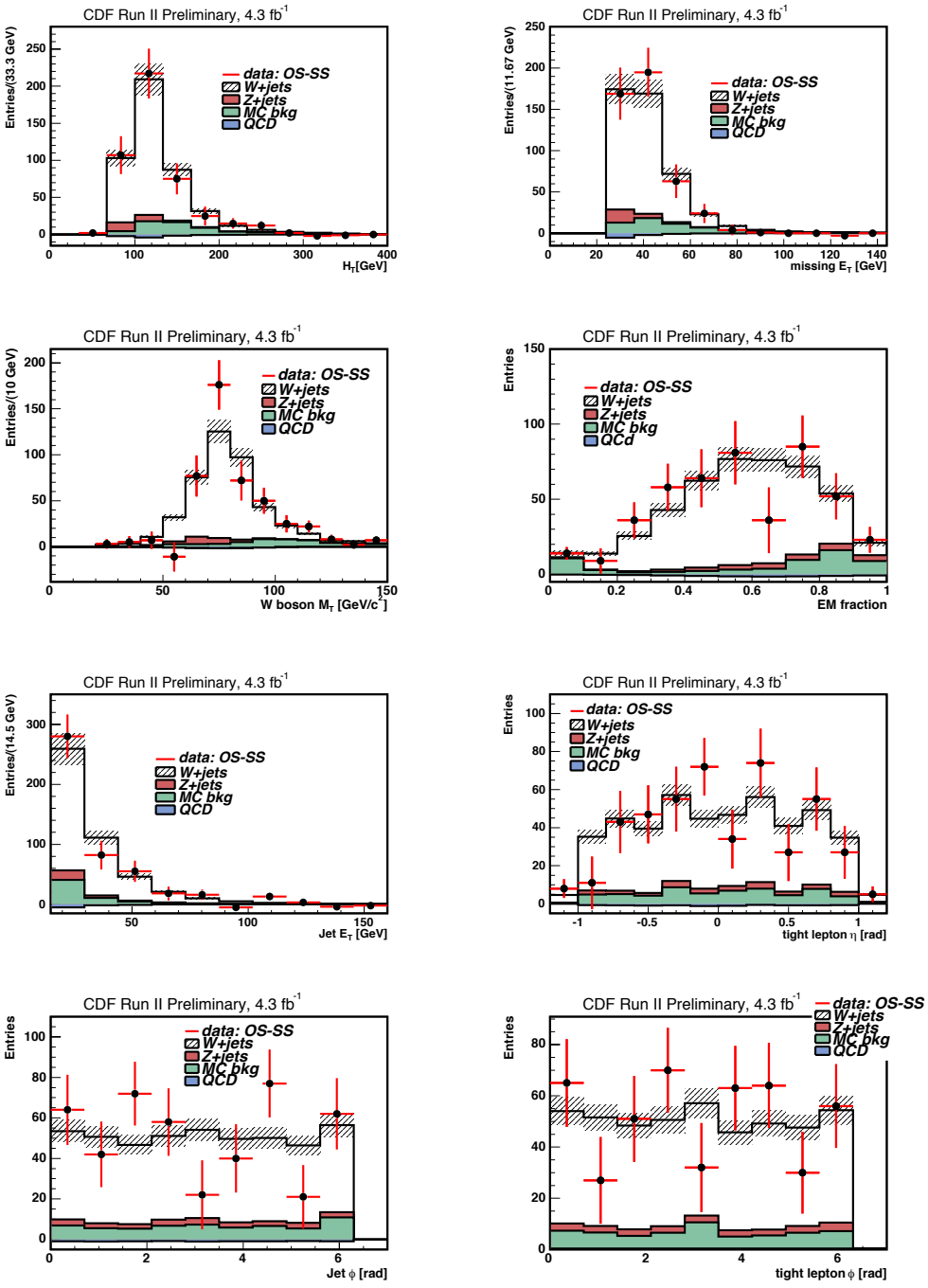

Figure 9: Kinematic plots of events tagged with the SLT$_\mu$. Each bin contains the difference between the number of opposite-sign and same-sign events.